LOCKHEED MARTIN ENERGY RESEARCH LIBRARIES
3 4456 0514601 7

CENTRAL RESEARCH LIBRARY
DOCUMENT COLLECTION

OAK RIDGE NATIONAL LABORATORY
operated by
UNION CARBIDE CORPORATION • NUCLEAR DIVISION
for the
U.S. ATOMIC ENERGY COMMISSION

ORNL-TM-3542

cy. 76

DETERMINATION OF THE FAST NEUTRON FLUX AND SPECTRUM IN THE OAK RIDGE BULK SHIELDING REACTOR WITH APPLICATION TO RADIATION DAMAGE EXPERIMENTS

J. D. Jenkins

OAK RIDGE NATIONAL LABORATORY
CENTRAL RESEARCH LIBRARY
DOCUMENT COLLECTION
LIBRARY LOAN COPY
DO NOT TRANSFER TO ANOTHER PERSON
If you wish someone else to see this document, send in name with document and the library will arrange a loan.
UCN-7969
(3 3-67)

NOTICE This document contains information of a preliminary nature and was prepared primarily for internal use at the Oak Ridge National Laboratory. It is subject to revision or correction and therefore does not represent a final report.

This report was prepared as an account of work sponsored by the United States Government. Neither the United States nor the United States Atomic Energy Commission, nor any of their employees, nor any of their contractors, subcontractors, or their employees, makes any warranty, express or implied, or assumes any legal liability or responsibility for the accuracy, completeness or usefulness of any information, apparatus, product or process disclosed, or represents that its use would not infringe privately owned rights.

ORNL-TM-3542

Contract No. W-7405-eng-26

Reactor Division

DETERMINATION OF THE FAST NEUTRON FLUX AND SPECTRUM IN THE OAK RIDGE BULK SHIELDING REACTOR WITH APPLICATION TO RADIATION DAMAGE EXPERIMENTS*

J. D. Jenkins

NOVEMBER 1971

*This work was performed for the Space Nuclear Propulsion Office under Purchase Order SNC-76.

OAK RIDGE NATIONAL LABORATORY
Oak Ridge, Tennessee 37830
operated by
UNION CARBIDE CORPORATION
for the
U. S. ATOMIC ENERGY COMMISSION

LOCKHEED MARTIN ENERGY RESEARCH LIBRARIES

3 4456 0514601 7

CONTENTS

	Page
Abstract	1
Introduction	1
Description of the Reactor and Experimental Facility	2
Calculations	4
Diffusion-Theory Calculation	6
One-Dimensional Transport-Theory Calculation	9
Two-Dimensional Transport-Theory Calculation	12
Experiment	18
Experimental Procedures	18
Data Analysis	19
Comparison of Calculation and Experiment	21
Calculation of Radiation Damage to Beryllium and Graphite	30
Analysis of Alternate, Lead-Shielded Facility	34
Spectrum Changes in the Altered Facility	35
Beryllium Damage Rates and Foil Activities in the Altered Facility	35
Acknowledgments	35
References	38

DETERMINATION OF THE FAST NEUTRON FLUX AND SPECTRUM IN THE OAK RIDGE BULK SHIELDING REACTOR WITH APPLICATION TO RADIATION DAMAGE EXPERIMENTS

J. D. Jenkins

Abstract

The fast neutron flux level and energy spectrum in the liquid nitrogen cryostat facility located at the north face of the Oak Ridge Bulk Shielding Reactor have been determined by the multiple foil activation technique and by calculation. Good agreement is obtained between the calculated and experimentally determined flux. The ratio of the integral fluxes above energy E given by calculation and experiment differ by less than 10% over the energy range from 1.86 eV to 10 MeV. In the course of the calculations a method was developed to utilize two-dimensional multigroup-transport calculations in a restricted area of the reactor core and simulate the rest of the reactor with appropriate boundary conditions. Calculated results using this technique gave better agreement with experiment than was obtained using one-dimensional transport calculations.

The spectrum so deduced was used to calculate relative radiation damage rates to beryllium. In addition, the calculational techniques verified by the detailed dosimetry experiment were used with confidence for the design of an alternate experimental facility and for the interpretation of data accumulated in it.

Keywords: radiation doses, spectra, radiation effects, beryllium, graphite.

INTRODUCTION

A series of irradiation experiments on selected NERVA materials is in progress in the Oak Ridge Bulk Shielding Reactor. The purpose of these experiments is to examine the behavior of the materials during and after irradiations by fast neutrons. The experimental apparatus is designed to permit irradiation of the materials at cryogenic temperatures (~80°K) and at room temperature, and to allow measurements to be made on the radiation induced changes to the electrical and thermal conductivities of the materials in situ at both the reduced temperature and after annealing.

The work described in this report was done in support of this irradiation program. It involves both a calculational and experimental effort directed at the accurate characterization of the neutron environment at the sample position and the use of these spectra to establish relative radiation damage rates to beryllium and carbon. Additional information on other aspects of the program is given in internal quarterly progress reports[1-3] and will be documented in final reports when the program is completed.

In any radiation damage experiment, two features of the neutron flux must be known in order to interpret the experimental results correctly. The first of these is the level of the neutron flux, that is, total number of neutrons per cm^2 per second passing through the target. In addition, since the ability of a neutron to cause damage depends to a large extent on its energy, one must know the spectrum or energy distribution of the neutron population.

Neither the neutron spectrum nor the total integrated flux is a readily measurable quantity in the environment near the core of an operating nuclear reactor. Hence a combination of calculations and dosimetry experiments is needed to determine the energy-dependence dose to the experimental sample. In addition, one would also like to be able to predict the sample dose independently by calculational techniques alone, both to gain added confidence in the dosimetry results and to verify the calculational methods which are involved in reducing the raw experimental data.

Both experimental and analytical techniques were employed in the determination of the neutron flux and spectrum at the face of the Bulk Shielding Reactor. A description of these two approaches and a comparison between the experimental and calculated results are given below.

DESCRIPTION OF THE REACTOR AND EXPERIMENTAL FACILITY

The Bulk Shielding Reactor (BSR) is a venerable swimming pool reactor constructed of MTR type[4] fuel elements suspended in a light-water reflector. A schematic of the reactor and its associated experimental facilities is given in Fig. 1. For the purpose of nuclear calculations

ORNL-DWG 67-4044

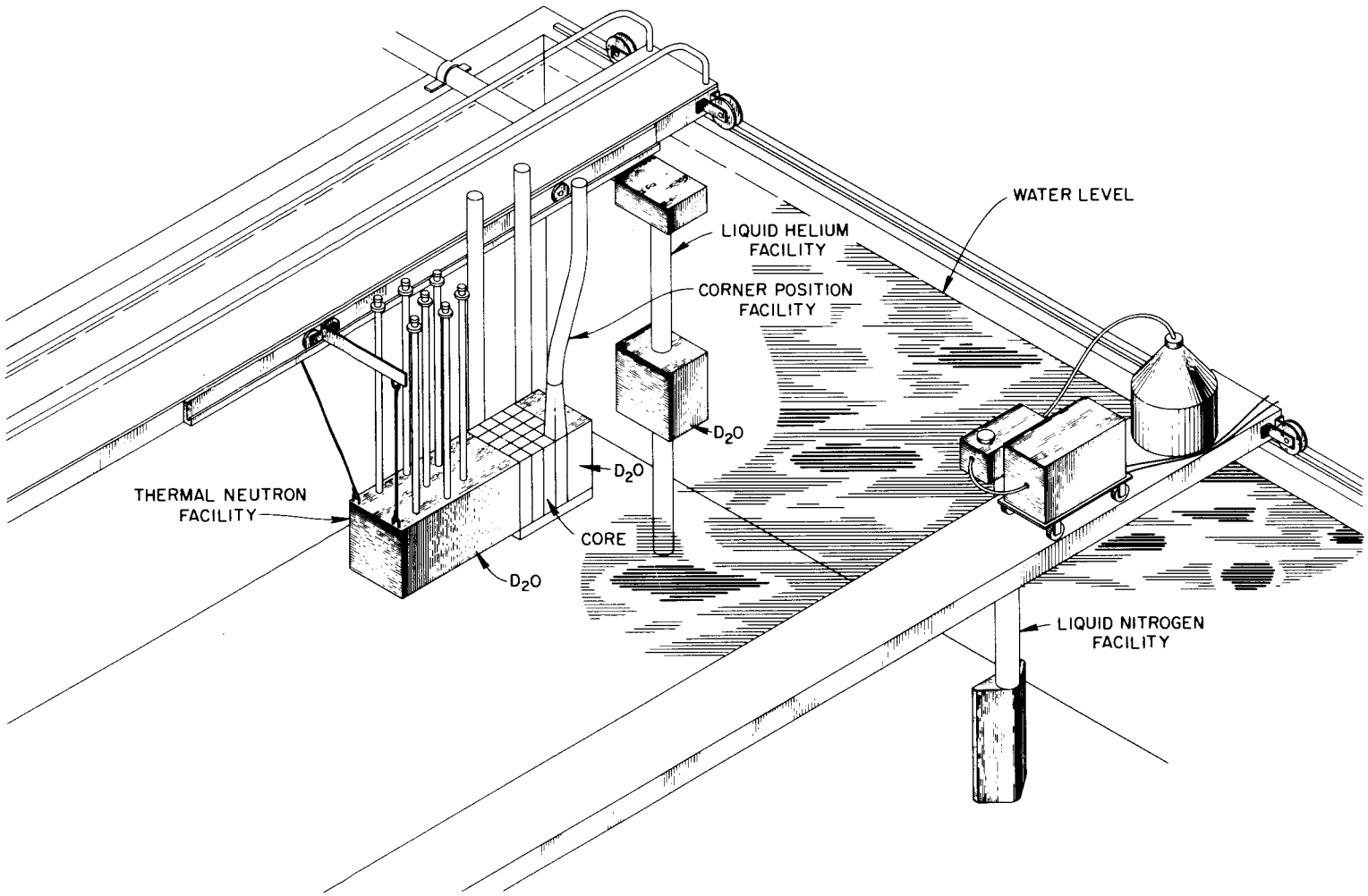

Fig. 1. Schematic of the Oak Ridge Bulk Shielding Reactor and experimental facilities.

it suffices to describe the facility as a light-water-moderated reactor with aluminum-clad enriched-uranium fuel arranged in plate-type elements with a metal-to-water ratio of about 0.72. A plan view of the reactor and its homogenized atom densities are given in Fig. 3 and Table 1 in the following section of this report. Additional details on the reactor design are available from a number of sources.[5,6]

The facility of particular interest in this work is the one labeled 'Liquid Nitrogen Facility' in Fig. 1. This facility consists of a hollow aluminum tube suspended from a movable bridge and held down by a triangular aluminum block which also serves as a mating plate when the facility is positioned adjacent to the reactor face.

The irradiation samples are centered in the tube at the reactor midplane. Figure 2 is a schematic of the sample holder and sample. Again, for this work, it is sufficient to note that the sample is located at the center of an essentially hollow tube and that the tube is separated from the reactor during irradiation by 1/2 in. of aluminum.

Figure 2 also indicates the location of a dosimeter well. Some of the data obtained in the preliminary dosimetry work described in this report were obtained from dosimeters irradiated in the dosimeter well. During the actual sample irradiations a few dosimeter materials are included in the well, which is accessible from outside, to provide consistency checks on the detailed dosimetry measurements described below.

CALCULATIONS

The objective of the calculational programs was to determine the neutron flux level and spectrum at the sample location solely by analysis. The program involved a detailed spatial calculation with a few energy groups to determine the flux level, and multigroup calculations, with relatively little spatial detail to establish the neutron energy distribution. In the course of the analysis questions arose as to the ability of the one-dimensional multigroup transport-theory calculations to correctly predict the neutron spectrum. A method was developed which permitted the use of more elaborate two-dimensional transport-theory multigroup calculations within the confines of computer capacity and running

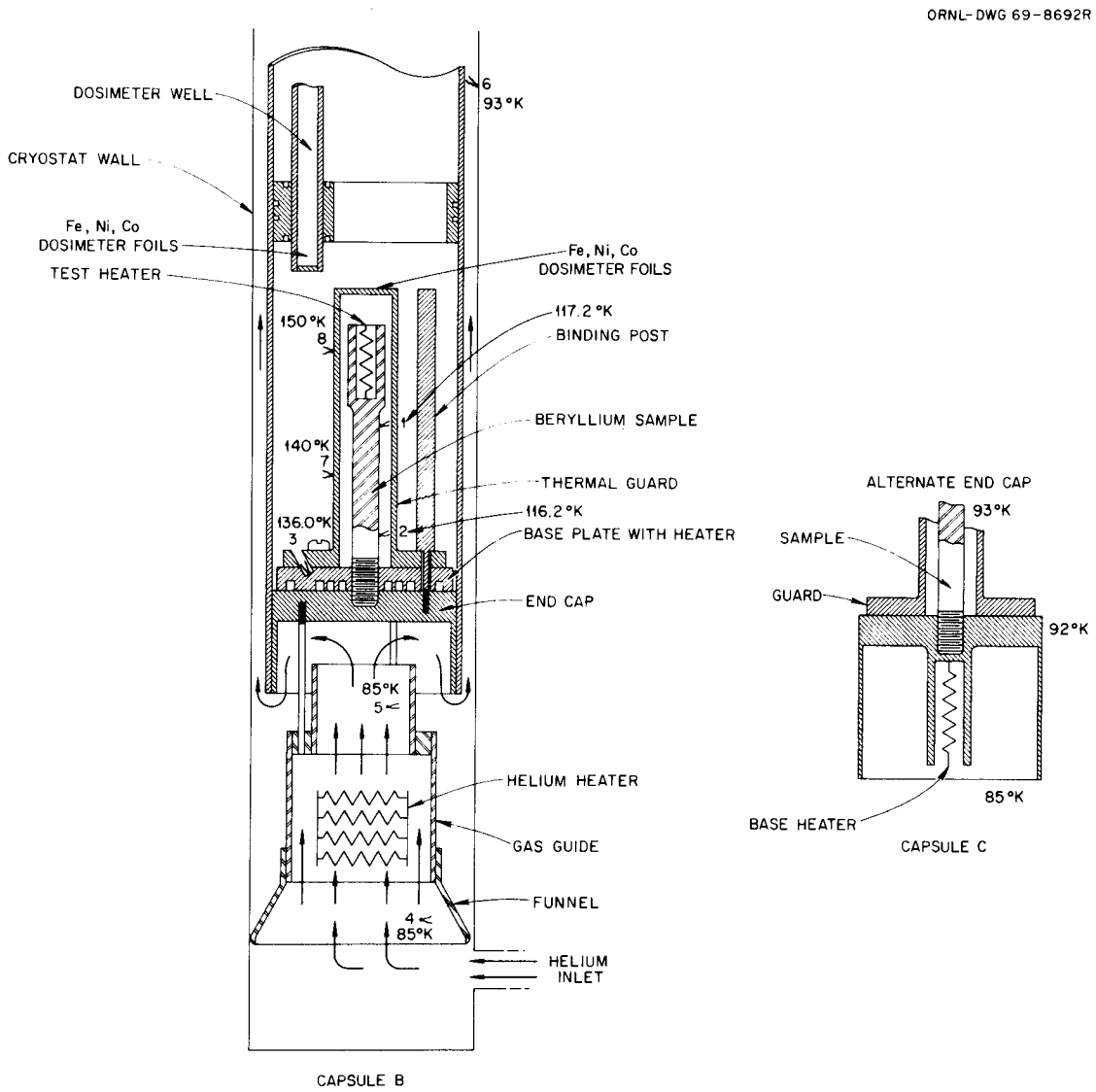

Fig. 2. Schematic of irradiation sample holder and sample.

times. This technique gave improved agreement between the calculated and measured spectra as will be described later.

Diffusion-Theory Calculation

As a first step in the analysis, a calculation was done to determine the neutron flux level at the sample position. Such a calculation requires a detailed representation of the spatial flux distribution. Computer storage limitations and running times dictate that such a calculation must be done using diffusion theory, the simplest representation for neutron transport. In addition, the energy description must be restricted to a small number of energy groups. A detailed two-dimensional diffusion-theory calculation was done with the computer code CITATION[7] using a seven-energy group (six fast and one thermal group) model. Group-averaged cross sections were obtained from the GAM[8] and THERMOS[9] programs.

A sketch of the calculational model is shown in Fig. 3. Thirty mesh increments were used in the horizontal direction and fifty in the vertical direction. Each fuel cell was represented explicity and fuel concentrations were calculated based on the then-current loading of the BSR. Control rods were represented explicitly and a poison search problem was run to adjust boron concentrations in the rod regions to yield a critical reactor. The model represents one-half of the actual system. A symmetry boundary condition was applied along the core centerline. Zero flux boundary conditions were applied at the outer three boundaries.

Table 1 lists the energy group structure and the homogenized atom densities input to the calculation.

The CITATION program will normalize calculated flux distributions to an arbitrary input reactor power level. In these calculations this factor was chosen based on an assumed reactor operating power level of 2 MW (the nominal power during sample irradiations). Thus the calculated fluxes represented absolute predicted flux levels. All subsequent calculated flux energy distributions and their comparison with experimental results are based on the absolute flux levels predicted by the CITATION calculation.

An independent experimental check was available for the diffusion-theory calculation and the normalization factor. The average thermal

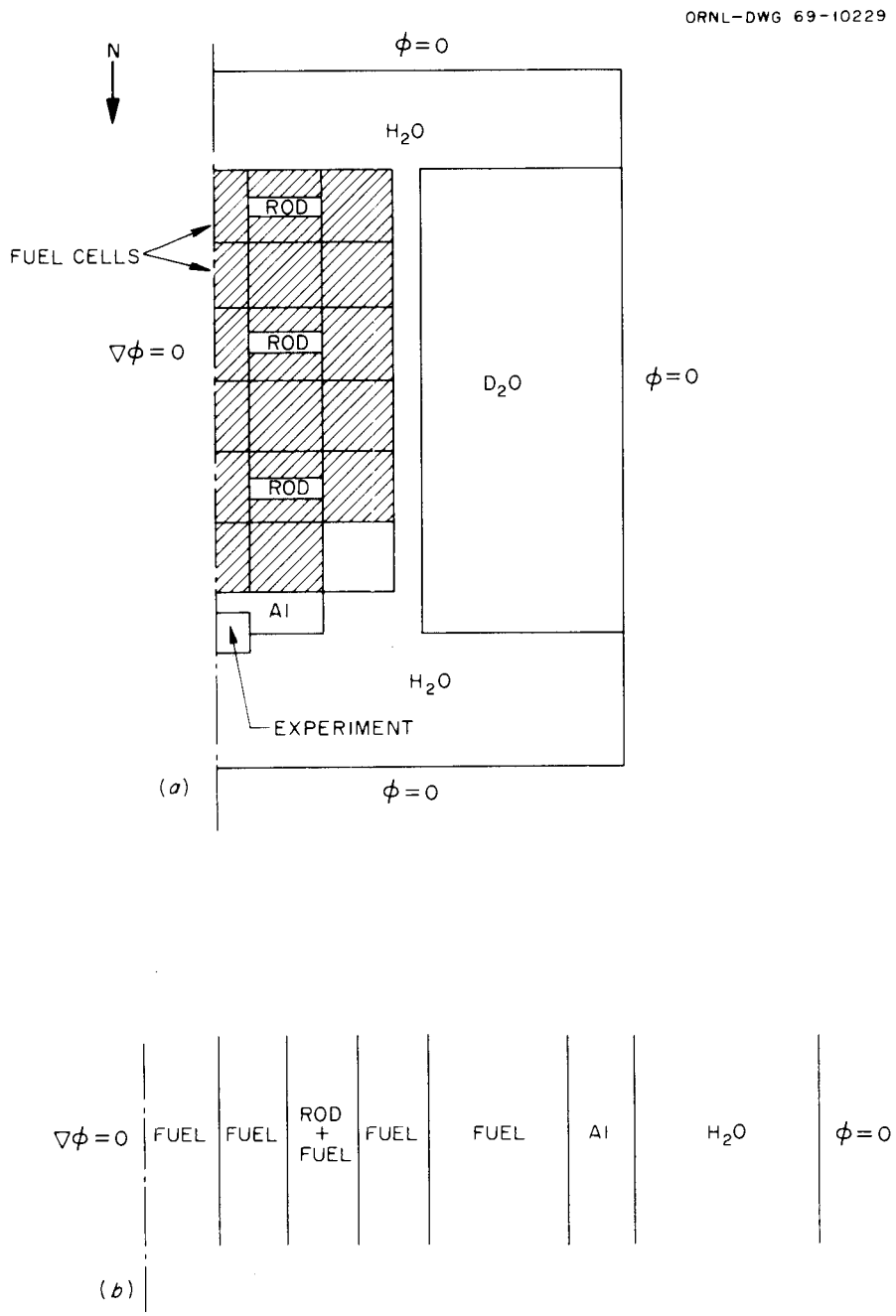

Fig. 3. Schematic of two-dimensional diffusion-theory calculational model and one-dimensional transport theory model.

Table 1. Energy Group Structure and Atom Densities Used in Diffusion-Theory Calculation

Group No.	Energy Group Structure	
	Upper Energy (eV)	Lower Energy (eV)
1	1.49×10^{7}	1.05×10^{6}
2	1.05×10^{6}	1.11×10^{5}
3	1.11×10^{5}	1.17×10^{4}
4	1.17×10^{4}	1.23×10^{3}
5	1.23×10^{3}	1.01×10
6	1.01×10	1.86
7	1.86	0.0

Element	Material Atom Densities, atoms/barn						
	Fuel	Control Rod	Blank Element	H_2O	D_2O	Aluminum	Experiment Tube
^{235}U	0.779×10^{-4} to 1.31×10^{-4} [a]						
^{238}U	8.03×10^{-6}						
Fe		3.18×10^{-2}					
Al	2.52×10^{-2}	1.50×10^{-2}	2.01×10^{-2}			$6.03 \times 10^{-}$	6.03×10^{-3}
B		1.98×10^{-4} [b]					
H	3.84×10^{-2}	2.48×10^{-2}	2.20×10^{-2}	6.61×10^{-2}			1.06×10^{-2}
O	1.92×10^{-2}	1.24×10^{-2}	1.10×10^{-2}	3.30×10^{-2}	3.30×10^{-2}		5.33×10^{-3}
D					6.61×10^{-2}		

[a] Varies for each fuel assembly.

[b] Boron density was search parameter in eigenvalue calculation.

flux in each fuel cell has been measured in the BSR core for this core loading.[10] These data, originally reported as 2200 m/sec fluxes were converted to integrated fluxes from 0 to 1.86 eV and are compared with the results of the diffusion calculation in Fig. 4. This comparison provides an independent check on the diffusion theory results and the absolute normalization of the calculation. Agreement is quite good and gives support to the calculated fast flux values at the experiment position.

One particular failing of the model is that the rectangular mesh forces one to represent the cylindrical experiment tube as a square region in the calculation. Unfortunately, this is the region of primary interest. It is difficult to assess the absolute effect of this misrepresentation, but experience with similar problems in other calculations leads one to believe that gross flux profiles and flux levels are insensitive to such an approximation as long as there are no strong absorbers in the distorted region.

One-Dimensional Transport-Theory Calculations

Detailed information on the neutron spectrum was initially obtained from a one-dimensional transport calculation. The model first chosen to represent the system is shown at the bottom of Fig. 3. It represents a traverse along the reactor north-south centerline. The calculation was run with the ANISN[11] program using S_8 quadrature, the GAM P_3 cross sections, and 100 energy groups.

The sample container and tube are not represented in the model. It was hoped that the spectrum would remain fairly constant across the aluminum plate region and that the average spectrum in the aluminum would be a good approximation to the actual spectrum in the capsule. The results of the calculation indicated that this was not a good assumption.

Figure 5 shows the variation across the plate of the effective cross sections for the ^{58}Ni(n,p) and ^{54}Fe(n,p) reactions as calculated with this model. These effective reaction cross sections, when defined as

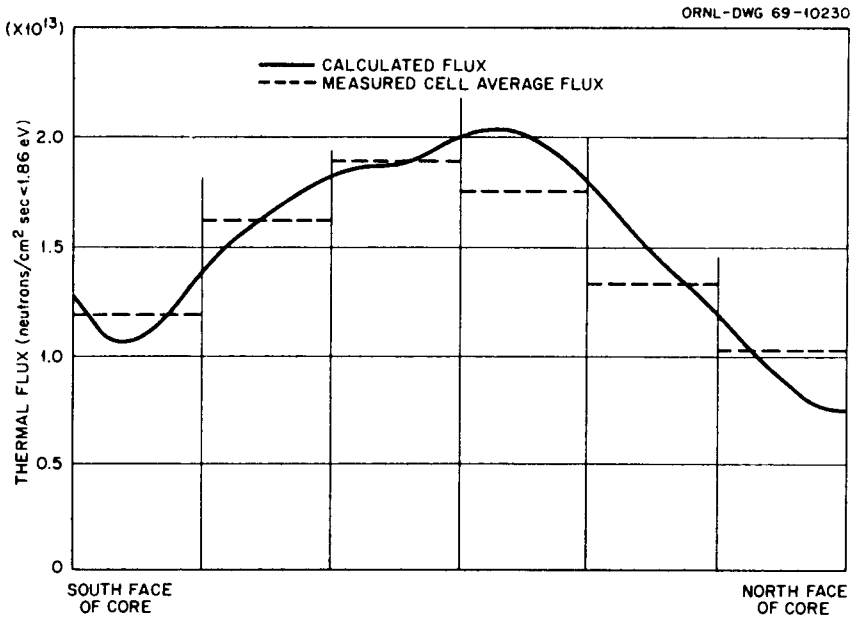

Fig. 4. Comparison of the measured and calculated thermal neutron flux along BSR centerline.

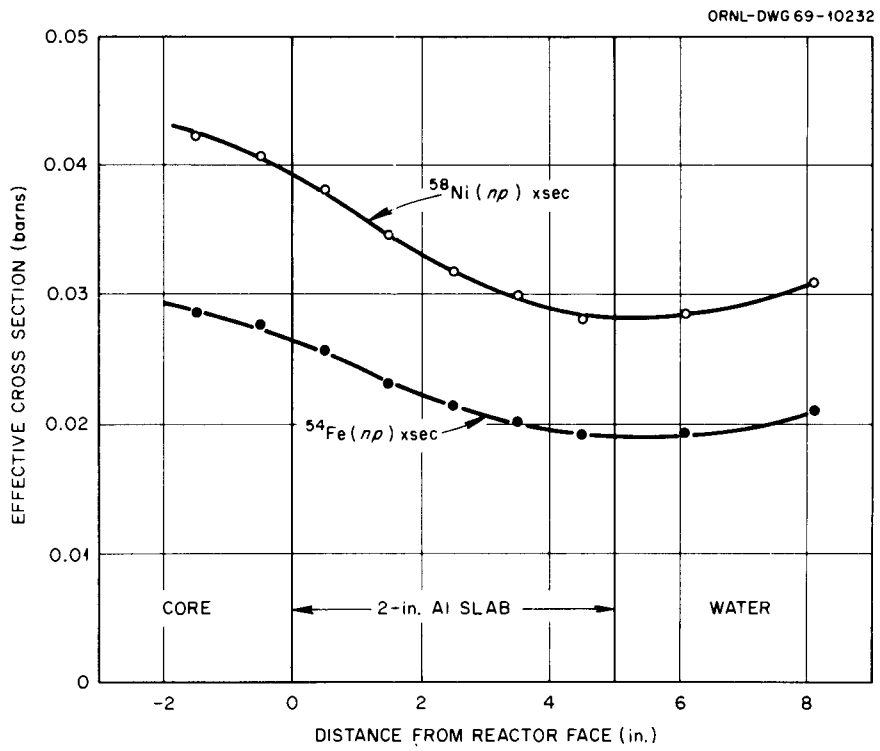

Fig. 5. Variation in calculated effective cross sections across aluminum region from one-dimensional transport calculation.

$$\bar{\sigma}_{eff}(x) = \frac{\int_{1.86\ eV}^{15\ MeV} \sigma(E)\ \phi(E,x)\ dE}{\int_{1.86\ eV}^{15\ MeV} \phi(E,x)\ dE},$$

are sensitive indicators of changes in the epithermal and high energy neutron distributions. Figure 5 indicates that the calculated effective cross sections vary by approximately 25% across the plate, implying a strong spectrum variation in this region and a resulting uncertainty as to which calculated spectrum one should chose as representative of that existing at the sample position.

For this reason, a second calculation was done using the model shown in Fig. 6. Here the experiment tube was represented by a void region. This removed the uncertainty introduced by the spatial variation of the spectrum (the spectrum is constant across the void) but left a lingering unease due to the possibility of two-dimensional spectrum effects not accounted for in the one-dimensional model.

Two-Dimensional Transport-Theory Calculation

The strong spatial variation of the spectrum observed in the one-dimensional transport calculations provided impetus to carry the calculational programs one step further. The most straightforward approach would have been to return to the diffusion-theory two-dimensional model, increase the number of energy groups to give additional detail in the high energy region, and run the problem with the two-dimensional transport program, DOT.[12] However this approach would have involved a prohibitively large amount of computer time. In addition, problems of this general type arise frequently enough in the analysis of irradiation experiments[13] to warrant the expenditure of some effort to develop a method particularly suited to their solution.

The approach taken was to represent the region of interest and its immediate surroundings in detail in two dimensions and approximate the remainder of the reactor by suitable boundary conditions around the outside of the extracted region. The approach is feasible for two reasons.

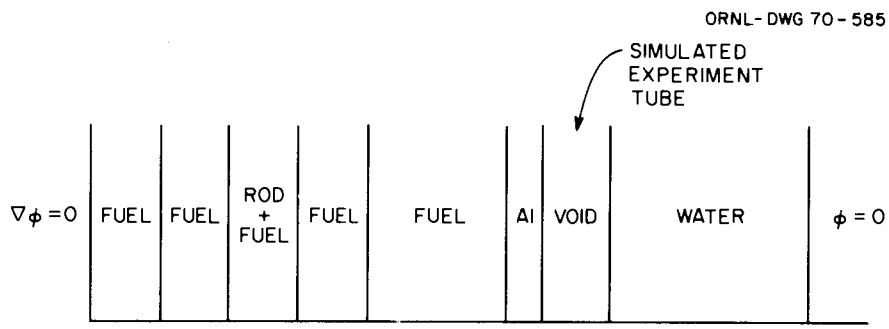

Fig. 6. Calculational model used in second one-dimensional transport theory calculation.

First, the boundary conditions are easily constructed from gross neutron balance considerations obtained from a more approximate calculation of the whole reactor system. Second, the solution in a localized region away from the boundaries is more sensitive to local effects than to detailed variations in sources located several mean free paths away, provided, of course, that the overall source strengths and gross distributions are correct.

For the BSR problem a gross solution for the whole reactor system was available from the diffusion-theory calculation. A subregion, pictured schematically in Fig. 7, was modeled for a 45-group DOT calculation with S_4 quadrature using the same spatial mesh as in the diffusion case and a somewhat broader group structure than was used for the one-dimensional case. The energy group structure for the one- and two-dimensional calculations is given in Table 2. The problem was run as a fixed source calculation with internal and boundary sources.

The boundary conditions and source can be constructed if one observes that the neutron population within any region of the reactor is composed of two classes: natives, who were born in the region and have never left, and visitors, who have crossed the region boundary from the outside. Under these definitions, a native venturing outside of the region is reclassified a visitor should he return. The neutron population in the region can then be simulated by providing a suitably distributed birth rate of natives within and visitors along the region boundary, together with a vacuum boundary condition on the outside.

The native birth rate is due entirely to neutron-producing reactions within the region. This is available from the fission distribution calculated in the diffusion-theory problem. Proper distribution in energy is achieved by assuming a fission spectrum for the internal distributed source.

The visitor source is also constructed from the diffusion problem. One observes that the number of neutrons per cm^2 flowing across a boundary can be expressed as a partial current. For example, across a boundary at y_o parallel to the x axis

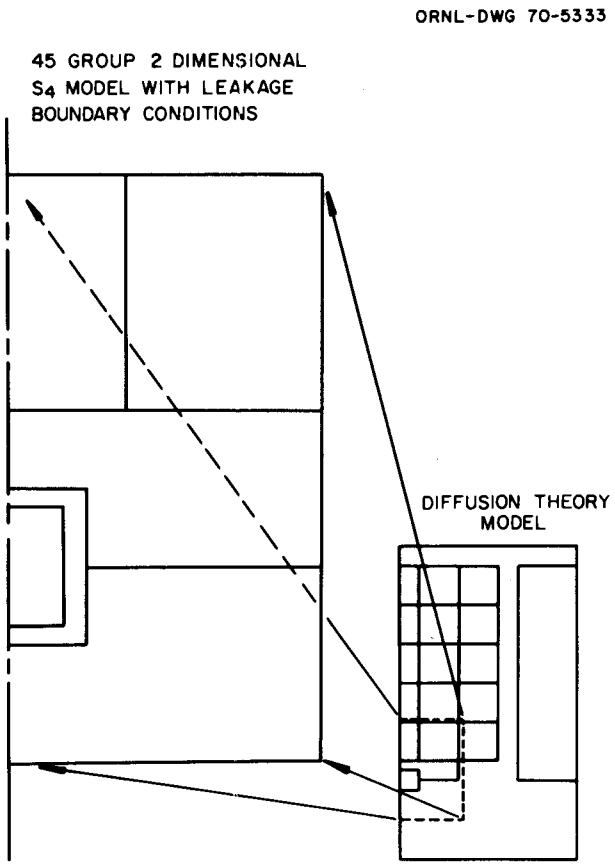

Fig. 7. Schematic showing two-dimensional transport model extracted from diffusion-theory model.

Table 2. Energy Group Structure for 45-Group DOT and 99-Group ANISN Calculations

ENERGY BOUNDARY	ANISN GROUP	DOT GROUP	ENERGY BOUNDARY	ANISN GROUP	DOT GROUP	ENERGY BOUNDARY	ANISN GROUP	DOT GROUP
0.14918E 08	1	1	0.55023E 06	34	27	0.15846E 04	67	38
0.13499E 08	2	2	0.49787E 06	35	28	0.12341E 04	68	39
0.12204E 08	3	3	0.45049E 06	36	28	0.96112E 03	69	39
0.11052E 08	4	4	0.40762E 06	37	29	0.74852E 03	70	39
0.10000E 08	5	5	0.36883E 06	38	29	0.58295E 03	71	39
0.90484E 07	6	6	0.33373E 06	39	30	0.45400E 03	72	40
0.81873E 07	7	7	0.30197E 06	40	30	0.35357E 03	73	40
0.74082E 07	8	8	0.27324E 06	41	31	0.27536E 03	74	40
0.67032E 07	9	9	0.24724E 06	42	31	0.21445E 03	75	40
0.60653E 07	10	10	0.22371E 06	43	31	0.16702E 03	76	41
0.54881E 07	11	11	0.20242E 06	44	32	0.13007E 03	77	41
0.49659E 07	12	12	0.18316E 06	45	32	0.10130E 03	78	41
0.44933E 07	13	13	0.16573E 06	46	32	0.78893E 02	79	41
0.40657E 07	14	14	0.14996E 06	47	33	0.61442E 02	80	41
0.36788E 07	15	15	0.13569E 06	48	33	0.47851E 02	81	42
0.33287E 07	16	16	0.12277E 06	49	33	0.37267E 02	82	42
0.30119E 07	17	17	0.11109E 06	50	34	0.29023E 02	83	42
0.27253E 07	18	18	0.86517E 05	51	34	0.22603E 02	84	42
0.24660E 07	19	19	0.67379E 05	52	34	0.17603E 02	85	42
0.22313E 07	20	20	0.52475E 05	53	35	0.13710E 02	86	43
0.20190E 07	21	21	0.40868E 05	54	35	0.10677E 02	87	43
0.18268E 07	22	21	0.31828E 05	55	35	0.83153E 01	88	43
0.16530E 07	23	22	0.24788E 05	56	36	0.64760E 01	89	43
0.14957E 07	24	22	0.19305E 05	57	36	0.50435E 01	90	43
0.13534E 07	25	23	0.15034E 05	58	36	0.39279E 01	91	44
0.12246E 07	26	23	0.11705E 05	59	36	0.30590E 01	92	44
0.11080E 07	27	24	0.91180E 04	60	37	0.23824E 01	93	44
0.10026E 07	28	24	0.71017E 04	61	37	0.18554E 01	94	44
0.90718E 06	29	25	0.55308E 04	62	37	0.14450E 01	95	44
0.82085E 06	30	25	0.43074E 04	63	37	0.11254E 01	96	45
0.74274E 06	31	26	0.33546E 04	64	38	0.87643E 00	97	45
0.67206E 06	32	26	0.26126E 04	65	38	0.68256E 00	98	45
0.60810E 06	33	27	0.20347E 04	66	38	0.53158E 00	99	45

$$J^{+}(x,y_o) = \frac{\phi(x,y_o)}{4} + \frac{D}{2}\frac{\partial\phi(x,y_o)}{\partial x}$$

or, in terms of the point value fluxes along the boundary, from the diffusion problem

$$J^{+}_{gk} = \frac{\phi_{ogk} + \phi_{igk}}{8} + \frac{D_{gk}}{2}\left(\frac{\phi_{ogk} - \phi_{igk}}{\Delta x}\right),$$

where

ϕ_{ogk} = the flux at the mesh interval outside the boundary,
ϕ_{igk} = theflux at the mesh interval inside the boundary,
Δx = the mesh spacing,
D_g = the diffusion coefficient,
g = a subscript denoting the diffusion theory broad-group number,
k = indicates position along the boundary.

It still remains to translate the partial incoming current into a suitable distributed source term and allocate the neutrons from the broad diffusion theory energy groups appropriately among the smaller groups of the transport problem.

The first objective was achieved by constructing a 0.1-cm-wide vacuum region around the outside of the transport model and assigning a distributed source of strength $20 \times J^{+}$ neutrons/cm^3 within it. This choice provides J^{+} neutrons crossing the boundary in an inward direction and a similar number escaping to the vacuum. The division of neutrons among the fine groups was accomplished by taking the average spectrum for the water, aluminum and fuel regions as calculated in the one-dimensional transport problem and using these spectra, where appropriate along the boundary, to distribute the source neutrons among the 45 transport theory groups. That is,

$$S_j = \frac{\sum_{i=N_j}^{M_j} \phi_i}{\sum_{i=N_g}^{M_g}} S_g ,$$

where

S_j = the boundary source in the jth group of the two-dimensional transport problem,

S_g = the source calculated from the inward-directed current in diffusion group g,

ϕ_i = the flux in group i of the one-dimensional transport problem in the appropriate medium,

N_j, M_j = the upper and lower groups from the one-dimensional problem contained within group j,

N_g, M_g = the upper and lower groups of the one-dimensional problem contained within group g.

The DOT problem was then run using the sources generated as described above. Results from this calculation are compared to those from the one-dimensional case and the multiple foil unfolding technique in the following section of this report.

EXPERIMENT

Experimental Procedures

Three separate dosimeter irradiations were carried out in the course of this study. In the first two, flux wires and quantz-encapsulated fissionable materials were used. The third irradiation used dime-sized foils of a number of different detector materials enclosed in a cadmium container.

In the first foil irradiation a dummy capsule similar to that pictured in Fig. 2 with a hollow sample was employed as a foil holder. In addition, foils were positioned on the near and far sides of the sample, relative to the reactor, to obtain a measure of the flux gradient in the vicinity of the capsule. The irradiation consisted of a two-hour run at 2-MW reactor power.

The second irradiation was conducted over a period of several days and a fairly complicated power history. In this run foils were located in a dummy sample at the capsule center and also in the dosimeter well to check for flux variations between sample and well positions.

The third irradiation was made using a special holder. The foils were stacked in a cadmium bucket with 100 mill walls. The holder was positioned at the reactor midplane at the center of the experiment tube and irradiated for 20 min at a reactor power of 209 kW.

Table 3 summarizes the materials included in each of the three foil irradiations.

Data Analysis

There are two basic approaches for the reduction of raw dosimeter data in the form of measured disintegrations per second per milligram of foil material to neutron flux data. Both require that the measured disintegration rates be reduced to saturated activities or reactions per detector atom per second during irradiation. This is achieved by the solution of the time-dependent chain equations governing the buildup and decay of radioactive nuclides using standard techniques.[14,15] At this point, two options are available.

First, one can assume that the neutron spectrum, $\phi(E)$, is known at the irradiation position from calculations. This spectrum, together with the energy-dependent reaction cross sections and saturated activities are used to obtain a flux level above energy E_c in the form

$$(\phi > E_c) = \frac{\text{Saturated Activity}}{\int_0^\infty \phi(E)\ \sigma(E) / \int_{E_c}^\infty \phi(E)} \qquad (1)$$

for each of the measured activations. If the resulting fluxes from a number of different detectors fall inside a band whose width is reasonable when compared to uncertainties in the reaction cross sections and in the measured disintegration rates, then one concludes that the calculated spectrum is acceptable and the derived flux level can be obtained from an average of the various detector results. Inconsistencies among a number of different detectors signals a poor representation for the neutron spectrum. Isolated inconsistencies point out possible counting errors or poorly known reaction cross sections.

Table 3. Foil Reactions Used in Dosimeter Irradiations

Foil Reaction	Run 1	Run 2	Run 3
$^{58}Ni(n,p)$	*	*	*
$^{54}Fe(n,p)$	*	*	*
$^{238}U(n,f)$	*		
$^{237}Np(n,f)$	*		
$^{27}Al(n,\alpha)$			*
$^{115}In(n,n')$			*
$^{56}Fe(n,p)$			*
$^{63}Cu(n,\gamma)$			*
$^{23}Na(n,\gamma)$			*
$^{35}Cl(n,\alpha)$			*
$^{46}Ti(n,p)$			*
$^{47}Ti(n,p)$			*
$^{48}Ti(n,p)$			*
$^{197}Au(n,\gamma)$			*
$^{32}S(n,p)$			*
$^{127}I(n,2n)$			*
$^{59}Co(n,\gamma)$			*

The second approach relies more heavily on the experimental activities and reaction cross sections. The implicit assumption is made that these are known more accurately than the spectrum can be calculated. Hence the experimental results are used to determine both the spectrum shape and level by adjusting both together to achieve agreement between the different detector results. That is, the integral fluxes defined by Eq. (1), above, as measured by different detectors, are forced into agreement by changes to the shape and level of $\phi(E)$. A number of techniques are available for performing this operation.[16,17] One danger in the application of the method is that a bad detector result can cause spurious adjustments to the spectrum if it is not spotted and eliminated before the fitting process.

Both of these techniques were used in the reduction of the BSR dosimeter data. The adjustment of the flux spectrum was done using the SAND-II program and detector cross-section library.[16] The same cross sections and the spectrum calculated with the two-dimensional transport-theory model were used to obtain flux levels by the first technique.

In both cases the SAND-II cross sections used to reduce the data from the third dosimeter irradiation were corrected to account for flux attenuation by the cadmium cover and, in the case of the resonance detectors, for resonance self-shielding within the individual foils. The self-shielding effect resulted in a reduction in the calculated effective cross sections for the resonance detectors of from 5 to 35%.

COMPARISON OF CALCULATION AND EXPERIMENT

A comparison between the fast flux obtained from the diffusion-theory calculation and from the dosimeters irradiated in the first two runs is shown in Fig. 8. The experimental activations were converted to fast flux values using cross sections averaged over the two-dimensional transport-theory spectrum. The figure shows the fast flux above 0.1 MeV. Good agreement is noted between the calculated flux level, which is based on an input power level, and the experimental flux at the capsule position. In addition, the calculation reproduces the measured gradient across the capsule fairly well.

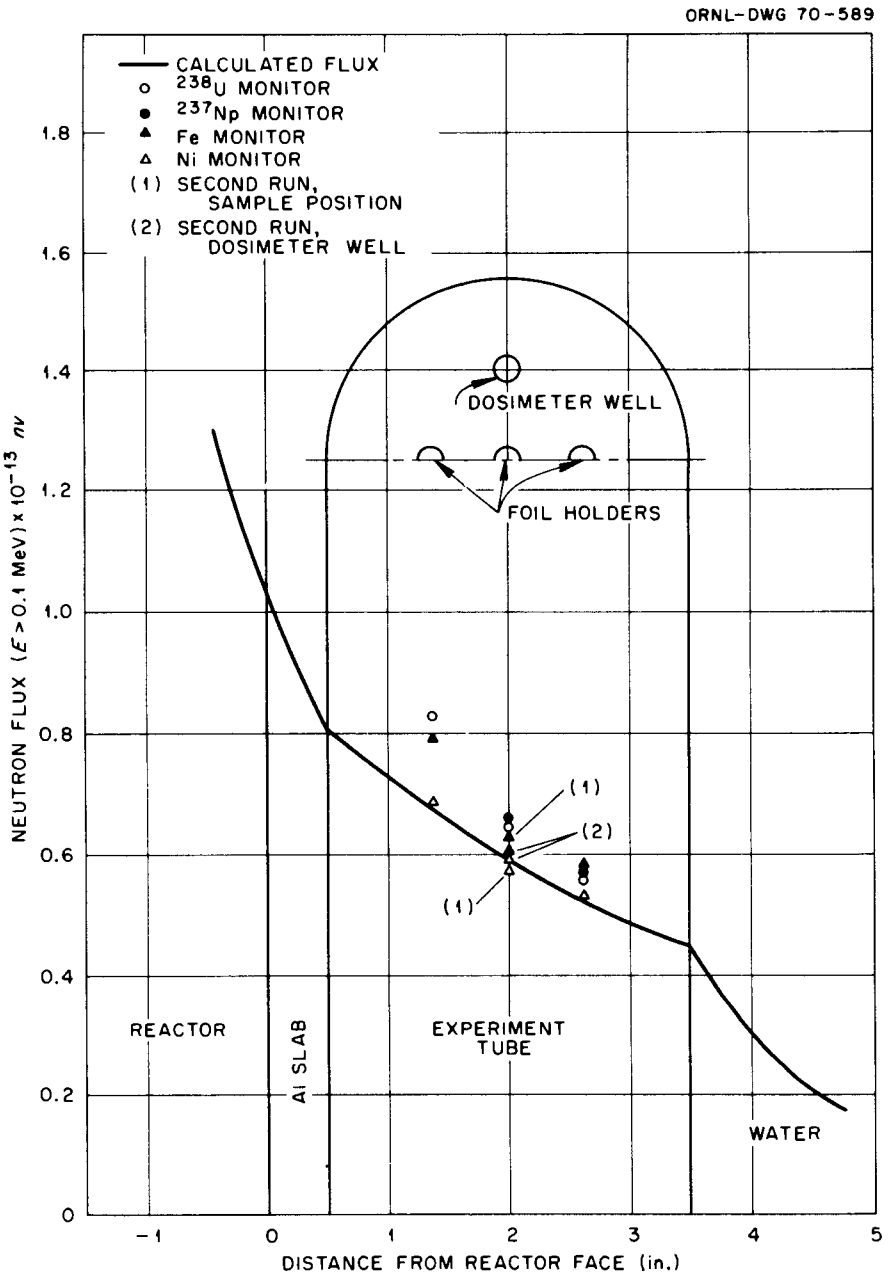

Fig. 8. Fluxes as determined from monitors and from diffusion theory.

It is particularly gratifying to note that the foils from the dosimeter well (labeled 2) and those from the sample position (labeled 1) gave similar results. This indicates that the foils in the dosimeter well will directly monitor the sample exposure during actual irradiations.

Figure 9 shows the results from all the dosimeters irradiated at the sample position in runs 1, 2 and 3. Again, these data have been represented as integrated fast flux above 0.1 MeV and the two-dimensional transport spectrum was used in the data reduction process. This same information is presented in Table 4 together with the measured saturated activities and the effective cross sections used in the data reduction. Table 4 also shows the effective cross sections obtained when the spectrum from the one-dimensional transport calculation was used for averaging, and the fluxes above 0.1 MeV resulting from their use in the data reduction process. For cases where more than one dosimeter of the same material was irradiated, Table 4 gives the average value.

The two-dimensional transport calculation yields a somewhat softer spectrum than the one-dimensional case with more neutrons in the 1/E tail. This difference is reflected in the effective cross sections listed in Table 4, the two-dimensional calculation giving somewhat lower effective cross sections for the high energy threshold reactions and higher cross sections for the resonance reactions.

A statistical analysis of the predicted fluxes using the two calculated spectra yields a derived one standard deviation of 13.4% for the results using the one-dimensional transport calculation and 11.6% using the more elaborate analysis. The implication is that the two-dimensional calculation yields a more accurate representation of the spectrum and this is reflected by the smaller variance in the independent results from the different dosimeter measurements.

As a second step in the analysis of the experimental data, the measured activities of the dosimeters were used, together with the energy-dependent cross sections, to generate a spectrum which reduced the deviations in the total fluxes predicted by the different dosimeters to a minimum. The SAND-II cross-section library and the SAND-II program were used in this analysis.

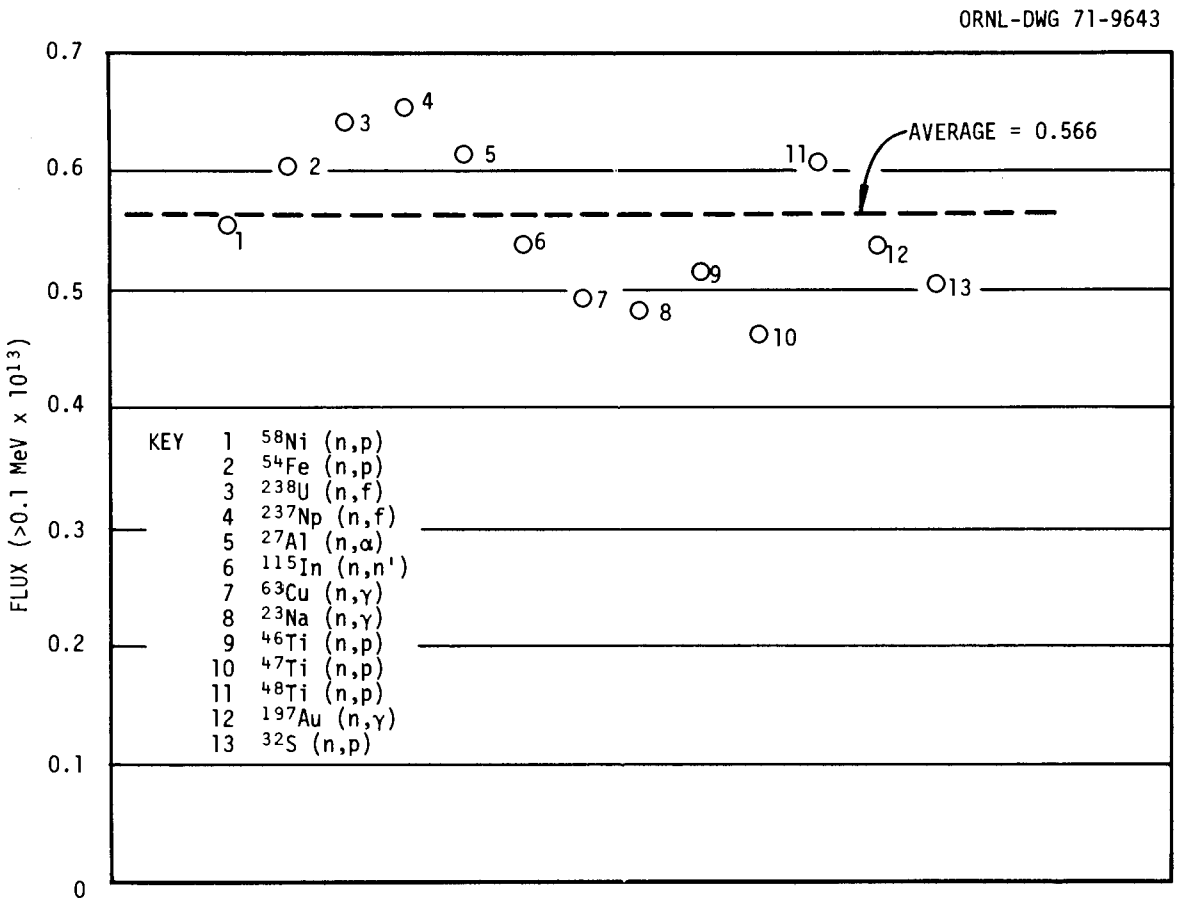

Fig. 9. Flux above 0.1 MeV as measured by each detector using two-dimensional transport theory calculated spectrum for cross section averaging.

Table 4. Flux Above 0.1 MeV and Effective Cross Sections Calculated Using One- and Two-Dimensional Transport Theory Models and Unfolded Spectrum

Reaction	Saturated Activity (dps/atom)	$\bar{\sigma}$ for $\phi > 0.1$ MeV Predicted Using Spectrum From			$\phi > 0.1$ MeV $\times 10^{12}$ Using $\bar{\sigma}$ Predicted with Spectrum at 2 MW		
		1-D Calculation	2-D Calculation	Unfolding	1-D Calculation	2-D Calculation	Unfolding
^{58}Ni(n,p)	4.01-13[a]	6.87-2	7.23-2	6.78-2	5.83	5.54	5.91
^{54}Fe(n,p)	3.11-13	4.65-2	4.91-2	4.97-2	6.40	6.04	6.25
^{238}U(n,f)	1.33-12	2.01-1	2.07-1	2.01-1	6.64	6.42	6.61
^{237}Np(n,f)	6.96-12	1.05	1.06	1.06	6.61	6.55	6.55
^{27}Al(n,α)	2.52-15	4.14-4	4.08-4	3.87-4	6.07	6.15	6.51
^{115}In(n,n')	7.30-13	1.32-1	1.35-1	1.37-1	5.53	5.38	5.32
^{56}Fe(n,p)	7.95-16	6.75-4[b]	--	--	11.78[b]	--	--
^{63}Cu(n,γ)	1.85-12	3.91-1	3.75-1	2.96-1	4.73	4.93	6.25
^{23}Na(n,γ)	9.82-14	2.07-2	2.04-2	1.57-2	4.73	4.80	6.25
^{35}Cl(n,α)	1.15-14	8.04-3[b]	--	--	14.31[b]	--	--
^{46}Ti(n,p)	4.68-14	8.51-3	9.10-3	7.15-3	5.50	5.14	6.54
^{47}Ti(n,p)	7.51-14	1.56-2	1.62-2	1.16-2	4.81	4.62	6.47
^{48}Ti(n,p)	7.99-16	1.34-4	1.30-4	1.34-4	5.94	6.09	5.96
^{197}Au(n,γ)	2.33-10	47.0	46.2	37.4	4.96	5.86	6.22
^{32}S(n,p)	2.65-13	3.82-2	4.01-2	4.00-2	6.95	5.04	6.62
^{127}I(n,2n)	4.27-16	3.88-4[b]	--	--	11.01[b]	--	--
^{59}Co(n,γ)	1.60-12	4.76[b]	--	--	3.36[b]	--	--
Average flux $\times 10^{13} \pm 1$ standard deviation					5.75± 0.77	5.58± 0.65	6.27± 0.37

[a]For 4.01-13 read 4.01×10^{-13}, etc.

[b]These reactions excluded from averages and unfolding calculations.

The spectrum-adjusting program requires an initial guess for the spectrum to be supplied at the start of the calculation. In this analysis the spectrum calculated with the one-dimensional transport model was used as a starting point for the spectrum adjustment. Figure 10 shows the initial spectrum guess and the final adjusted spectrum which minimized the deviations between the different detector results. The calculated spectrum in Fig. 10 is normalized to the total fast flux predicted by the diffusion calculation and the adjusted curve is normalized to the experimental dosimeter results. The ratio of the calculated integral flux above energy E to the unfolded or experimental integral flux above the same energy is also shown at the top of Fig. 10. That is, the figure shows

$$R(E) \equiv \frac{\int_E^\infty \phi(E)_{\text{calculated}}}{\int_E^\infty \phi(E)_{\text{experimental}}} .$$

It must be emphasized that the unfolded or experimental spectrum is not entirely independent of the initial guess supplied to the program. Thus the fine structure which appears in Fig. 10 is a reflection of similar structure present in the input spectrum. It has been demonstrated,[18] however, that gross spectrum shifts, in this case the visible softening of the adjusted spectrum, are consistently reproduced for any "reasonable" input guess and that the final unfolded spectrum can be reproduced to ±5% despite variations in the starting point. In this regard, it is worth pointing out that an "unreasonable" guess can sometimes lead to nonphysical solutions due to instabilities in the fitting program.

A final comparison between the computed integral spectra and the unfolded spectra is given in Fig. 11. Here the ratio of the integral spectrum above energy E as calculated by the one- and two-dimensional transport calculations to the unfolded spectrum is shown. It is seen that the two-dimensional calculation gives better agreement with the unfolded spectrum over the entire energy range. Table 5 displays the same information from the two-dimensional calculation and the unfolding method in numerical form.

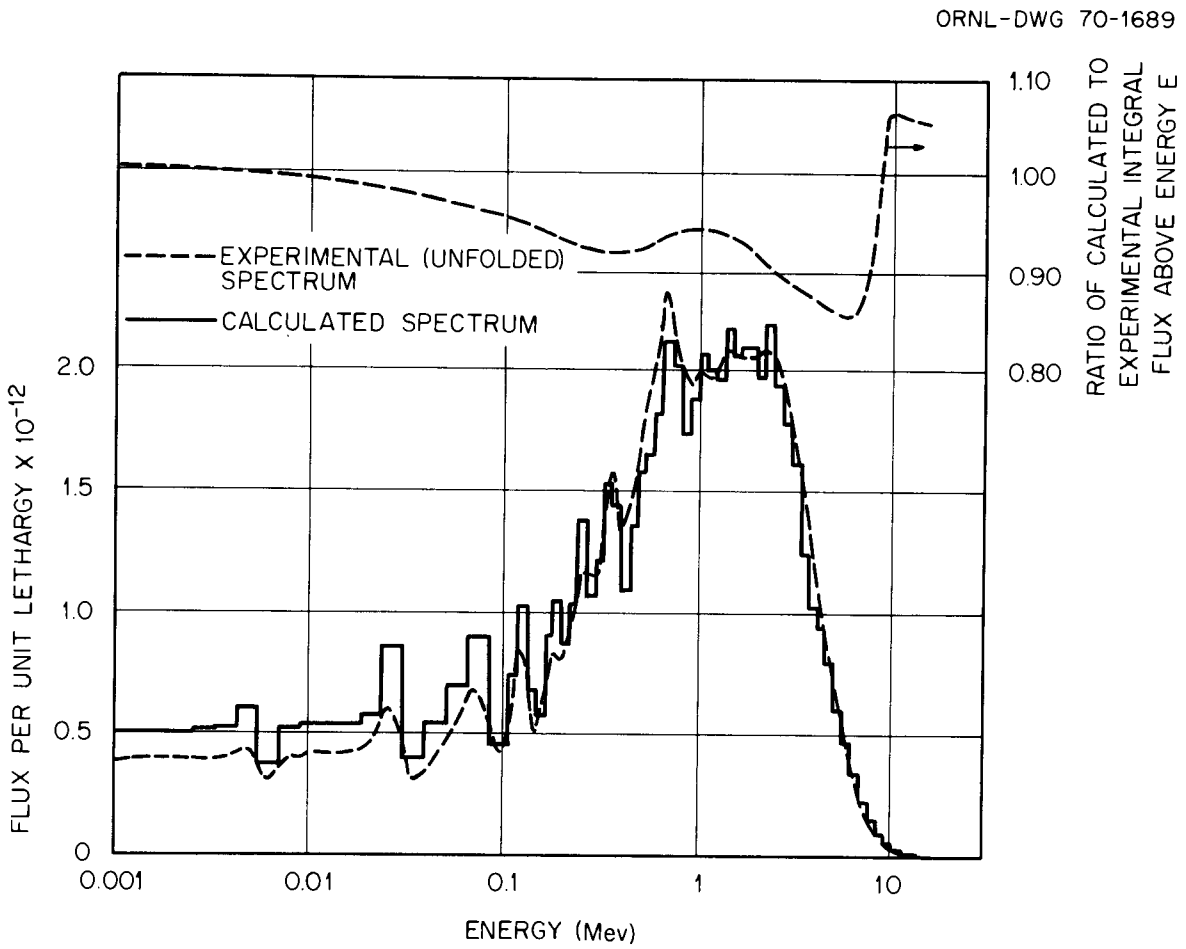

Fig. 10. Comparison of unfolded spectrum and spectrum calculated with one-dimensional transport theory model.

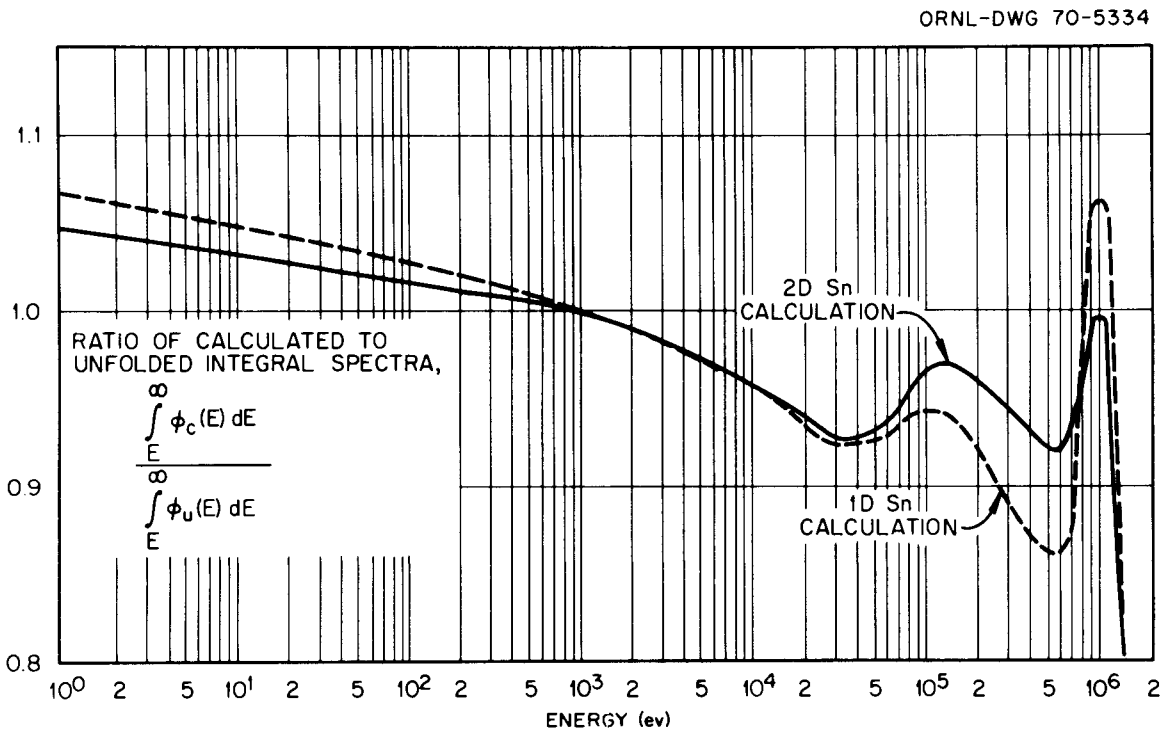

Fig. 11. Comparison of calculated and experimental integral fluxes.

Table 5. Final Integral Flux Values Above Energy E from Calculation and Experiment at 2 MW Reactor Power

Energy (eV)	Flux Above Energy E from Calculation	Flux Above Energy E from Unfolding
1.10×10^{7}	0.160×10^{10}	0.162×10^{10}
5.4×10^{6}	0.148×10^{12}	0.167×10^{12}
1.0×10^{6}	0.305×10^{13}	0.317×10^{13}
8.2×10^{5}	0.342×10^{13}	0.357×10^{13}
5.5×10^{6}	0.416×10^{13}	0.444×10^{13}
1.8×10^{5}	0.585×10^{13}	0.585×10^{13}
1.1×10^{5}	0.592×10^{13}	0.620×10^{13}
2.5×10^{4}	0.686×10^{13}	0.696×10^{13}
9.1×10^{3}	0.738×10^{13}	0.741×10^{13}
5.8×10	0.869×10^{13}	0.852×10^{13}
0.414	1.202×10^{13}	1.125×10^{13}

A standard deviation has been estimated from the flux monitor results reduced with the spectra calculated with the one- and two-dimensional models. The standard deviation was estimated from the expression

$$\sigma^2 = \frac{\sum_{i=1}^{n} (\bar{\phi} - \phi_i)^2}{(n - 1)} ,$$

where $\bar{\phi} = \sum_{i=1}^{n} \phi_i/n$ and ϕ is the flux above 0.1 MeV.

The results from this calculation are given in Table 4. The flux monitor results indicate that the flux level above 0.1 MeV has been measured to better than ±6% using the spectrum unfolding technique and the comparison between the calculated and unfolded spectra, Fig. 11, indicates that the spectrum shape is also known to ±10% over the entire energy range.

CALCULATION OF RADIATION DAMAGE TO BERYLLIUM AND GRAPHITE

The flux spectrum measurements and calculations described above can be combined with a damage cross section for beryllium or graphite to determine the damaging ability of the Bulk Shielding Reactor spectrum relative to the spectrum in the NERVA engine reflector.

Energy transfer kernels, $\sigma_s(E)\ K(E,T)$, were constructed for use in calculating radiation damage in beryllium and graphite.[19] The kernels describe the probability that a neutron with energy E will produce a primary recoil atom with energy T. The kernels are based on scattering cross section and angular distribution information contained in the Evaluated Nuclear Data Files (ENDF/B).[20]

Possession of the kernels makes it a simple matter to calculate primary recoil atom spectra in varying neutron spectra. In addition, the kernels plus a suitable secondary displacement model, $\nu(T)$, allows calculation of damage cross sections in the form

$$D(E) = \int_0^\infty \sigma_s(E)\ K(E,T)\ \nu(T)\ dT\ .$$

Here D(E) is the number of displacements per atom and unit flux of neutrons with energy E, and $\nu(T)$ is the secondary displacement model which gives the total number of displacements caused by a primary recoil with energy T. The calculated damage cross section for beryllium using the Lindhard model[21-23] to describe secondary displacements is shown in Fig. 12.

The relative damaging ability of a given flux spectrum, $\phi(E)$, can now be calculated by evaluating the expression:

$$\text{Relative damage per unit flux} = \frac{\int_0^\infty \phi(E)\ D(E)\ dE}{\int_0^\infty \phi(E)\ dE}\ .$$

The relative damage per unit fast flux above a given energy, E_c, can be calculated from the expression

$$\text{Relative damage per unit flux above } E_c = \frac{\int_0^\infty \phi(E)\ D(E)\ dE}{\int_{E_c}^\infty \phi(E)\ dE}\ .$$

This second definition is necessary when one wants to compare radiation damage in different spectra and the total exposures are reported in terms of "fast flux greater than E_c MeV." It is a stratagem contrived to conform to current practices in reporting fast neutron exposures.

A value of 1 MeV has been chosen as the cutoff for reporting fast neutron dose in the current series of beryllium damage experiments in the BSR. Calculations have been run to evaluate the relative damaging ability of the spectrum in the BSR experimental facility and the spectrum in the reflector of the system of interest. The present best representation of the experimental facility spectrum, shown in Fig. 10, and a coarse mesh spectrum supplied by Westinghouse for the NERVA reflector, shown in Fig. 13, were used in the calculation. The results for beryllium

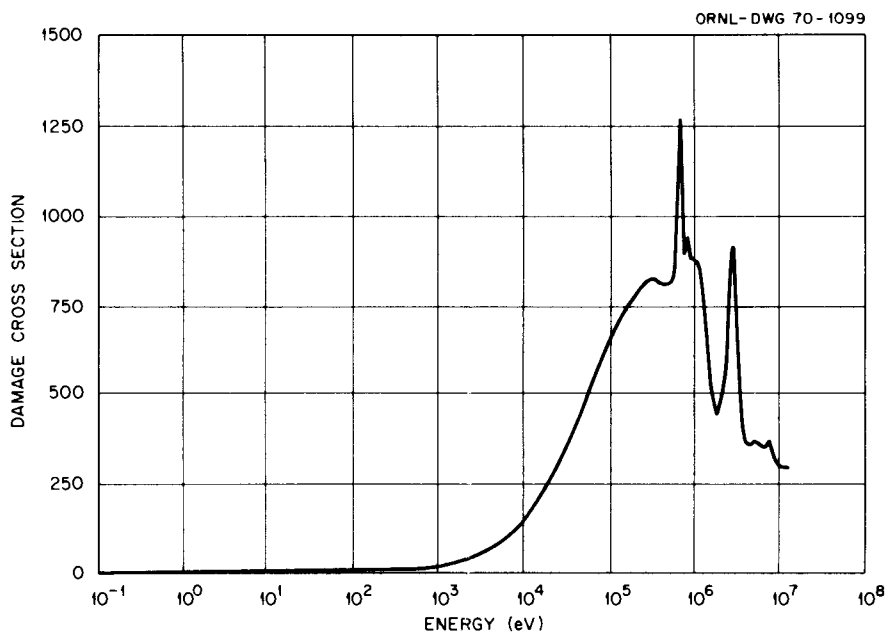

Fig. 12. Damage cross section in displacements per atom per unit flux versus energy for beryllium.

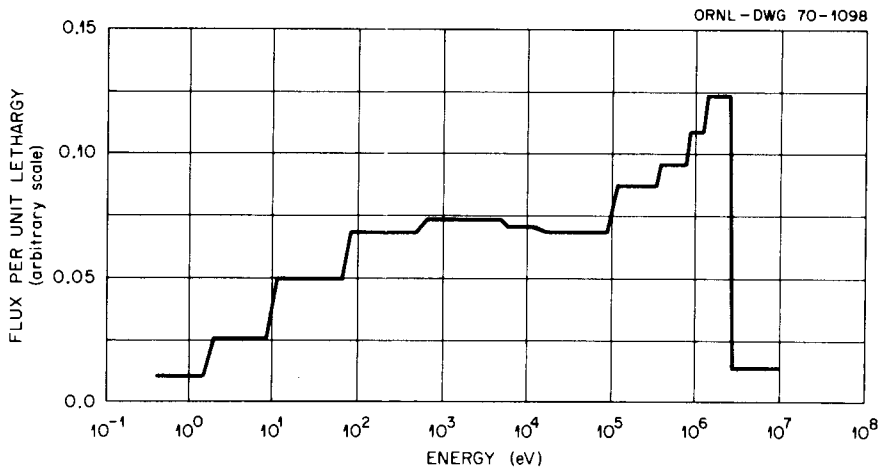

Fig. 13. Neutron spectrum for NERVA reflector.

and graphite are presented in Table 6 below. These results indicate that the reflector spectrum is 1.4 times more damaging than the experiment spectrum for beryllium and 1.3 times more damaging for graphite if the dose is measured in terms of flux of energy greater than 1 MeV. In more practical terms this means that to simulate a dose of 1.0×10^{19} neutrons/cm^2 ($E > 1.0$ MeV) in the actual system one must irradiate beryllium to a dose of 1.4×10^{19} neutrons/cm^2 in the BSR, and graphite to a dose of 1.3×10^{19} neutrons/cm^2 ($E > 1.0$ MeV).

Table 6. Relative Damaging Ability of BSR and Reflector Spectra Per Unit Flux Above 1 MeV

Reactor spectrum	Relative damage per atom unit flux > 1 MeV $\times 10^{-24}$	
	Be	C
BSR experiment	1650	1240
NERVA system reflector	2310	1590

ANALYSIS OF ALTERNATE, LEAD-SHIELDED FACILITY

Subsequent to the calculations and experiment described above, it was decided that the gamma heat load to the cryostat facility could be substantially reduced by surrounding the tube with approximately 1 in. of lead shielding. It was necessary to determine if such a shield would have a detrimental effect on the fast neutron dose at the sample position, thus offsetting any gains in cryostat cooling capabilities by requiring longer irradiations to achieve the same equivalent damage to the samples. With the confidence inspired by the preceding calculational and experimental program, it was felt that this question, and the resulting beryllium damage rates in the altered facility, could be determined primarily with calculational methods.

Spectrum Changes in the Altered Facility

One-dimensional, 99-group transport calculations similar to those described earlier were done to determine the fast neutron spectrum shifts in the lead shielded facility. The spectrum resulting from the presence of the lead is compared to the unshielded facility spectrum in Fig. 14. Note that the spectrum in the shielded facility is considerably softer than that obtained previously. This can be explained by the effect of the inelastic scattering in the lead shield. The calculations also indicated only a small reduction in the integral flux above 0.1 MeV due to the presence of the shield.

Beryllium Damage Rates and Foil Activities in the Altered Facility

The spectrum calculated for the altered facility was used to estimate the damage rate to beryllium in the manner described above. In addition, two dosimeters, an iron wire and a nickel wire, were irradiated in the lead shielded configuration, and these data were converted to flux above 0.1 MeV, using the new calculated spectrum.

The results of these calculations are shown in Tables 7 and 8. The effect of the spectrum shift is to reduce the effective activation cross sections of the dosimeters and increase the effective damage cross section to the beryllium. The sparse dosimeter data indicate a reduction in the flux above 0.1 MeV by about 15% and the spectrum shift causes an increase to the beryllium damage rate of about 5% with a net decrease to the predicted damage accumulation rate to beryllium of about 10%. These results have also been confirmed by the in-pile monitoring of the beryllium property changes which indicate little or no change to the neutron induced damage to beryllium due to the presence of the lead shield.

ACKNOWLEDGMENTS

The author wishes to thank J. M. Williams and N. E. Hinkle for their assistance in the design and performance of the foil irradiation experiments, F.B.K. Kam for assistance in performing the SAND-II calculations, W. T. Mullins for his assistance in counting the dosimeters, and S. S. Hurt for providing descriptive data on the BSR facility.

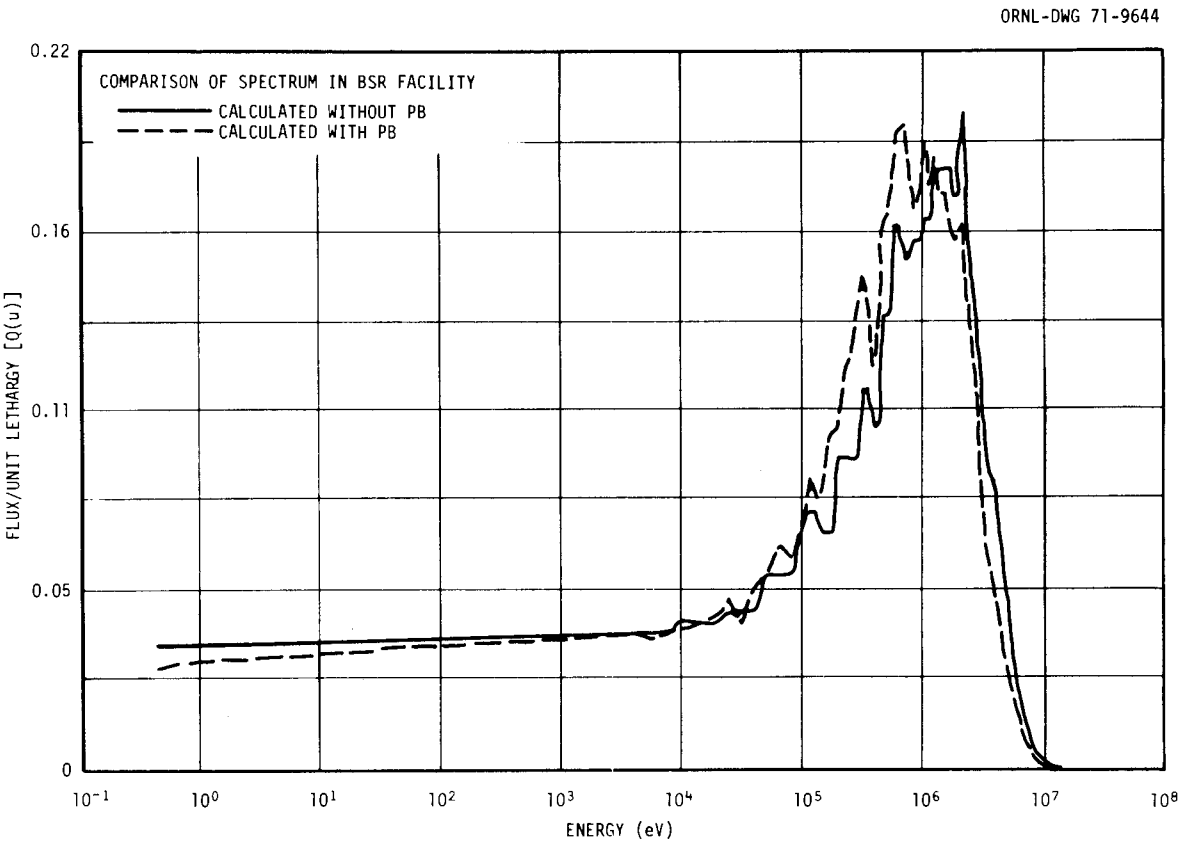

Fig. 14. Comparison of spectra in lead shielded and unshielded cryostat tubes.

Table 7. Effective Cross Sections for Flux >0.1 MeV for Old (Unshielded) and New (Shielded) Configurations

Cross Section	$\bar{\sigma}(\phi>0.1$ MeV) Unshielded Configuration (barns)	$\bar{\sigma}(\phi>0.1$ MeV) Shielded Configuration (barns)	$\frac{\bar{\sigma}\text{ Shielded Configuration}}{\bar{\sigma}\text{ Unshielded Configuration}}$
$^{54}Fe(n,p)$	0.0492	0.0326	0.66
$^{58}Ni(n,p)$	0.0723	0.0498	0.69
Be damage (displacements/ atom $\times 10^{24}$)	700	732	1.046

Table 8. Flux Predicted by Fe and Ni Dosimeters in Unshielded and Shielded Configurations

[Reactor power = 2 MW(t)]

Dosimeter	Flux, >0.1 MeV Unshielded	Flux, >0.1 MeV Shielded	$\frac{\phi_{shielded}}{\phi_{unshielded}}$
$^{58}Ni(n,p)$	5.54×10^{12}	4.58×10^{12}	0.82
$^{54}Fe(n,p)$	6.04×10^{12}	5.54×10^{12}	0.92

REFERENCES

1. W. P. Eatherly, Irradiation Effects in Selected NERVA Materials: Progress Report for March-June 1969, Oak Ridge National Laboratory, unpublished internal document, Sept. 1969.

2. W. P. Eatherly, Irradiation Effects in Selected NERVA Materials: Progress Report for July-September 1969, Oak Ridge National Laboratory, unpublished internal document, January 1970.

3. W. P. Eatherly, Irradiation Effects in Selected NERVA Materials: Progress Report for September, 1969-January 1970, Oak Ridge National Laboratory, unpublished internal document, August 1970.

4. A. M. Weinberg, T. E. Cole, and M. M. Mann, The Materials Testing Reactor and Related Research Reactors, Proceedings of the International Conference on the Peaceful Uses of Atomic Energy, Geneva, 1955, Vol. 2, pp. 402-419, United Nations, New York, 1956.

5. C. E. Klabunde and B. C. Kelley, Irradiation Facilities in the Oak Ridge National Laboratory Bulk Shielding Reactor, Proceedings of Symposium on Developments in Irradiation Capsule Technology, Pleasonton, Calif, May 1966, TID-4500 (CONF-660511).

6. W. M. Breazeale, The New Bulk Shielding Facility at ORNL, USAEC Report ORNL-991, Oak Ridge National Laboratory, May 1951.

7. T. B. Fowler and D. R. Vondy, Nuclear Reactor Core Analysis Code: CITATION, USAEC Report ORNL-TM-2496, Oak Ridge National Laboratory, July 1969.

8. G. D. Joanou and J. S. Dudek, GAM-II: A B_3 Code for the Calculation of Fast Neutron Spectra and Associated Multigroup Constants, GA-4265, General Atomic, Sept. 1963.

9. H. C. Honeck, THERMOS: A Thermalization Transport Theory Code for Reactor Lattice Calculations, USAEC Report BNL-5826, Brookhaven National Laboratory, Sept. 1961.

10. S. S. Hurt, Oak Ridge National Laboratory, personal communication to J. D. Jenkins, Oak Ridge National Laboratory.

11. W. W. Engle, ANISN: A One-Dimensional Discrete Ordinates Transport Code, USAEC Report K-1693, Union Carbide Corporation, Nuclear Division, 1967.

12. F. R. Mynatt, A User's Manual for DOT, USAEC Report K-1694, Union Carbide Corporation, Nuclear Division, 1968.

13. J. D. Jenkins, A Technique for the Neutronics Analysis of In-Pile Irradiation Experiments (to be published).

14. R. D. Evans, The Atomic Nucleus, McGraw-Hill, New York, 1955.

15. W. C. Morgan, Foils: A Program for Computing Neutron Exposures from Foil Activation Data, USAEC Report HW-81367, April 1964.

16. W. N. McElroy et al., A Computer Automated Iterative Method for Neutron Flux Spectra Determination by Foil Activation, I, II, III, and IV, AFWL-TR-67-41, Sept. 1967.

17. G. Di Cola and A. Rota, Calculation of Differential Fast Neutron Spectra from Threshold Foil Activation Data by Least Squares Series Expansion Method, Nucl. Sci. Eng. 23; 344 (1965).

18. W. N. McElroy, Nucl. Sci. Eng., 36: 109 (1969).

19. J. D. Jenkins, Nucl. Sci. Eng., 41: 155 (1970).

20. H. C. Honeck, Specifications for an Evaluated Nuclear Data File for Reactor Applications, USAEC Report BNL-50066, Brookhaven National Laboratory, 1966.

21. J. Lindhard, V. Nielsen, and Scharff, Kgl. Danske Videnskab. Selskab, Mat.-Fys. Medd., 36, No. 10 (1968).

22. J. Lindhard, M. Scharff, and H. E. Schiott, Kgl. Danske Videnskab. Selskab, Mat.-Fys. Medd., 33, No. 4 (1963).

23. J. Lindhard et al., Kgl. Danske Videnskab. Selskab, Mat.-Fys. Medd., 33, No. 10 (1963).

Internal Distribution

1. H. F. Bauman
2. S. E. Beall
3. L. L. Bennett
4. D. S. Billington
5. E. E. Bloom
6. E. G. Bohlmann
7. G. E. Boyd
8. J. E. Carr
9. H. C. Claiborne
10. C. E. Clifford
11. J. A. Conlin
12. W. B. Cottrell
13. J. A. Cox
14. F. L. Culler, Jr.
15. G. W. Cunningham
16. J. E. Cunningham
17. J. G. Delene
18-22. W. P. Eatherly
23. T. B. Fowler
24. A. P. Fraas
25. J. H. Frye
26. B. L. Greenstreet
27. W. R. Grimes
28. P. N. Haubenreich
29. N. E. Hinkle
30. H. W. Hoffman
31. F. J. Homan
32. S. S. Hurt
33-37. J. D. Jenkins
38. F.B.K. Kam
39. P. R. Kasten
40. H. T. Kerr
41. R. T. King
42. M. I. Lundin
43. R. N. Lyon
44. R. E. MacPherson
45. F. C. Maienschein
46. H. C. McCurdy
47. D. L. McElroy
48. A. J. Miller
49. J. M. Napier, Y-12
50. A. R. Olsen
51. P. Patriarca
52. A. M. Perry
53. B. E. Prince
54. G. L. Ragan
55. M. W. Rosenthal
56. J. L. Scott
57. M. R. Sheldon
58. M. J. Skinner
59. O. L. Smith
60. I. Spiewak
61. D. Steiner
62. D. A. Sundberg
63. J. H. Swanks
64. W. E. Thomas
65. M. L. Tobias
66. D. B. Trauger
67. D. R. Vondy
68. A. M. Weinberg
69. J. R. Weir
70. F. G. Welfare
71. G. D. Whitman
72. M. K. Wilkinson
73. J. M. Williams
74. F. J. Witt
75. F. W. Young
76-77. Central Research Library
78. Y-12 Document Reference Section
79-81. Laboratory Records Department
82. Laboratory Records Department, LRD-RC

External Distribution

83. J. W. Allen, CAD, Forth Worth, Texas 76100
84. C. M. Cox, WADCO Corp., Richland, Washington 99352
85. R. E. Dahl, Pacific Northwest Laboratory, P. O. Box 999, Richland, Washington 99352
86-88. J. A. Demastry, WANL, Pittsburgh, Pa. 15236
89-90. J. E. Drennan, Battelle Memorial Institute, Columbus, Ohio 43201

91. I. L. Helms, Space Nuclear Systems Office, Washington, D. C. 20545
92. H. Hessing, Space Nuclear Systems Office, Washington, D. C. 20545
93-95. J. J. Lombardo, Space Nuclear Systems Office, Cleveland Extension, Cleveland, Ohio 44135
96. D. P. MacMillian, Los Alamos Scientific Laboratory, Los Alamos, Mexico 87544
97. W. N. McElroy, Pacific Northwest Laboratory, P. O. Box 999, Richland, Washington 99352
98. T. P. Merrick, WANL, Pittsburgh, Pa. 15236
99. R. E. Nightingale, Battelle Northwest, P. O. Box 999, Richland, Washington 99352
100-101. T. Redfield, ANSC, Sacramento, Calif. 95801
102. G. S. Richmond, P. O. Box 1, Orford, New Hampshire 03777
103. A. D. Rossin, Argonne National Laboratory, 9700 South Cass Ave., Argonne, Ill. 60439
104. W. S. Scheib, Space Nuclear Systems Office, Washington, D. C. 20545
105-106. A. F. Schmidt, National Bureau Standards, Boulder, Colo. 80302
107. R. W. Schroeder, SNPO-C, Cleveland, Ohio 44135
108. C. F. Schwenk, Space Nuclear Systems Office, Washington, D. C. 20545
109. J. Taub, Los Alamos Scientific Laboratory, Los Alamos, Mexico 87544
110. H. H. Yoshikawa, Pacific Northwest Laboratory, P. O. Box 999, Richland, Washington 99352
111-112. Division of Technical Information Extension (DTIE)
113. Laboratory and University Division, ORO
114-116. Director, Division of Reactor Licensing, USAEC, Washington, D. C. 20545
117-118. Director, Division of Reactor Standards, USAEC, Washington, D. C. 20545
119-123. Executive Secretary, Advisory Committee on Reactor Safeguards, USAEC, Washington, D. C. 20545